AGU PUBLICATIONS

JGR

Journal of Geophysical Research: Atmospheres

RESEARCH ARTICLE
10.1002/2013JD021139

Key Points:
- We implement the first GCM diagnostic calculation of cryosphere radiative effect
- Global average CrRE from snow and sea ice is -4 W m^{-2} in present-day simulations
- Earth absorbs 1.6 W m^{-2} more insolation from cryosphere loss by 2099 in RCP8.5

Correspondence to:
J. Perket,
perketj@umich.edu

Citation:
Perket, J., M. G. Flanner, and J. E. Kay (2014), Diagnosing shortwave cryosphere radiative effect and its 21st century evolution in CESM, *J. Geophys. Res. Atmos.*, *119*, 1356–1362, doi:10.1002/2013JD021139.

Received 4 NOV 2013
Accepted 16 JAN 2014
Accepted article online 17 JAN 2014
Published online 15 FEB 2014

Diagnosing shortwave cryosphere radiative effect and its 21st century evolution in CESM

Justin Perket[1], Mark G. Flanner[1], and Jennifer E. Kay[2]

[1]Department of Atmospheric, Oceanic and Space Sciences, University of Michigan, Ann Arbor, Michigan, USA, [2]Department of Atmospheric and Ocean Sciences, University of Colorado at Boulder, Boulder, Colorado, USA

Abstract We incorporate a new diagnostic called the cryosphere radiative effect (CrRE), the instantaneous influence of surface snow and sea ice on the top-of-model solar energy budget, into two released versions of the Community Earth System Model (CESM1 and CCSM4). CrRE offers a more climatically relevant metric of the cryospheric state than snow and sea ice extent and is influenced by factors such as the seasonal cycle of insolation, cloud masking, and vegetation cover. We evaluate CrRE during the late 20th century and over the 21st century, specifically diagnosing the nature of CrRE contributions from terrestrial and marine sources. The radiative influence of ice sheets and glaciers is not considered, but snow on top of them is accounted for. Present-day global CrRE in both models is -3.8 W m^{-2}, with a boreal component (-4.2 to -4.6 W m^{-2}) that compares well with observationally derived estimates (-3.9 to -4.6 W m^{-2}). Similar present-day CrRE in the two model versions results from compensating differences in cloud masking and sea ice extent. Over the 21st century, radiative forcing in the Representative Concentration Pathway (RCP) 8.5 scenario causes reduced boreal sea ice cover, austral sea ice cover, and boreal snow cover, which all contribute roughly equally to enhancing global absorbed shortwave radiation by 1.4–1.8 Wm^{-2}. Twenty-first century RCP8.5 global cryospheric albedo feedback are +0.41 and +0.45 W/m^2/K, indicating that the two models exhibit similar temperature-normalized CrRE change.

1. Introduction

Realistic portrayal of cryospheric change is critical for accurate climate change modeling. In addition to the strongly positive snow/ice albedo feedback, where increasing temperatures decrease cryospheric coverage, warmer temperatures also darken snow and sea ice through thinning, accelerated metamorphism, and increased melt pond coverage. After cloud and water vapor feedback, surface albedo feedback is the third strongest global positive feedback mechanism [e.g., *Bony et al*., 2006; *Soden and Held*, 2006]. Snow area fraction and sea ice extent are important metrics often used to evaluate models, but do not capture the cryospheric radiative influence, which is modulated by factors such as seasonal insolation, cloudiness, vegetation cover, ground albedo, melt pond distribution, and impurity content in snow.

To quantify these influences, we incorporate a new diagnostic in the Community Earth System Model (CESM): the cryosphere radiative effect (CrRE). CESM includes sophisticated snow and sea ice physics, making it a suitable candidate for such development. The ice model includes ponding and multiple subgrid ice thickness categories, while the multilayer snow model accounts for metamorphosis, compaction, and vegetation burial [*Lawrence et al*., 2011; *Holland et al*., 2012] Both models apply two-stream radiative transfer models to calculate albedo and account for embedded light-absorbing aerosols [*Briegleb and Light*, 2007; *Flanner et al*., 2007].

Analogous to the cloud radiative effect [e.g., *Ramanathan et al*., 1989; *Arking*, 1991; *Stephens*, 2005], CrRE is defined as the instantaneous influence of surface snow and sea ice on the top-of-model (TOM) shortwave energy budget [*Flanner et al*., 2011], TOM being nearly equivalent to the top of the atmosphere. CrRE incorporates the influences of vegetation masking and sea ice ponding on albedo, as well as insolation variation and shortwave attenuation and scattering by clouds, aerosols, and gases. Longwave cryospheric effects are not included here, though they may also be important. Although broadband emissivities of cryospheric and noncryospheric surfaces are similar, snow and ice can insulate the ground or facilitate substantial cooling of the skin surface, thereby reducing outgoing longwave radiation. Estimation of longwave effects, however, requires calculation of temperature feedback in the absence of snow and thus cannot be accomplished through an instantaneous framework.

©2014. American Geophysical Union. All Rights Reserved.

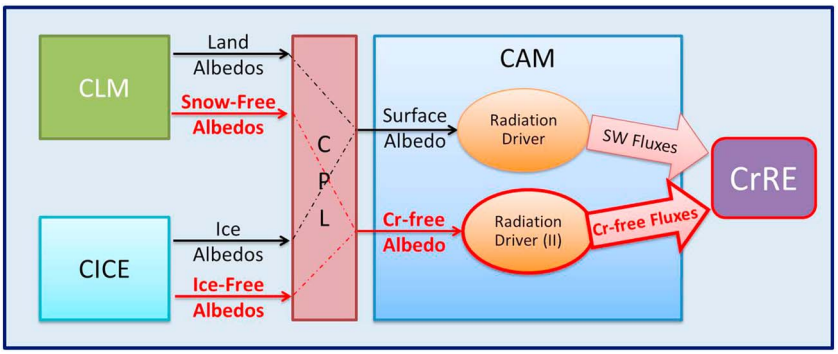

Figure 1. Diagram of CrRE computation. CLM, CICE, and CAM are CESM's land, sea ice, and atmosphere models, respectively, while CPL is the coupler software connecting component models. Additions to the CESM code are highlighted in red.

In addition to providing the exact shortwave influence of the cryosphere, the CrRE diagnostic can be used to evaluate the accuracy of assumptions applied in surface albedo feedback analysis. For example, the radiative kernel method has been applied in several analyses of albedo feedback [e.g., *Shell et al.*, 2008; *Soden et al.*, 2008; *Donohoe and Battisti*, 2011; *Flanner et al.*, 2011; *Qu and Hall*, 2013], but the importance of consistency between atmospheric fields used to generate kernels and nonlinearities in top-of-atmosphere flux change with albedo changes larger than 0.01 (the typical perturbation) have not been rigorously evaluated.

2. Methods

2.1. Diagnostic CrRE Calculation

We implemented the diagnostic CrRE calculations in CESM versions 1.0.5 and 1.1.1 [*Gent et al.*, 2011; *Hurrell et al.*, 2013]. CESM contains the Community Land Model (CLM), the Community Ice Code (CICE) model, the Parallel Ocean Program (POP), and the Community Atmosphere Model (CAM), among other components, synchronized through a coupler. CrRE was calculated by extracting, at each time step, snow-free albedo from CLM and ice-free ocean albedo from CICE, passing these states through the coupler (CPL) to the atmosphere model, and conducting parallel atmospheric radiative transfer calculations with the true and cryosphere-free surface albedos (Figure 1). The difference in TOM net shortwave flux between these calculations provides the cryosphere radiative effect. Note that open-ocean albedo is calculated by default in the coupler, not POP. When sea ice is present, CICE computes albedo. For the purposes of CrRE, we incorporated this open-water albedo formalism into CICE, identical to how CESM would treat ice-free ocean. CESM partitions surface albedo into four components: direct visible, diffuse visible, direct near-IR, and diffuse near-IR. Merging of land, ocean, and sea ice albedos is handled consistently for both sets of surfaces. Over glaciers and ice sheets, CrRE represents the influence of overlying snow relative to bare ice, which in CESM has constant visible and near-IR albedos of 0.80 and 0.55, respectively. This diagnostic therefore offers a description of the fast feedback (snow and sea ice) component of the cryosphere. While ice sheets clearly provide large capacity for altering planetary albedo over long timescales, estimation of their radiative influence requires involved assumptions of how the ice sheet-free albedo is related to vegetation cover, isostatic rebound, and sea level.

2.2. Model Simulations

We conducted two fully coupled 21st century simulations driven by the Representative Concentration Pathway 8.5 (RCP8.5) forcing scenario with the CrRE diagnostic enabled, using CAM4 in CESM 1.0.5 (i.e., CCSM4; using the B_RCP8.5_CN component set) and CAM5 in CESM 1.1.1 (B_RCP8.5_CAM5_CN component set) [*Meinshausen et al.*, 2011]. These hybrid runs used year 2007 initial conditions from existing RCP8.5 experiments, and progressed to year 2100. This allowed us to evaluate evolution of snow and ice radiative influence in response to strong warming, simulated by different model versions. We also conducted 10 year present-day simulations (B_2000_CN component set) with CAM4 physics in CESM 1.0.5 and CAM5 in CESM 1.1.1 for comparison with observationally derived estimates of CrRE. These runs were allowed a 1 year spin-up period before data were taken for analysis. All simulations were conducted at $0.9 \times 1.25°$ horizontal resolution.

©2014. American Geophysical Union. All Rights Reserved.

Table 1. All- and Clear-Sky Cryosphere Radiative Effect (Watts Per Square Meter)[a]

		Present Day				Twenty-First Century RCP 8.5[b]		
Model Version	Region	Total	Glacial Land	Sea Ice	Nonglacial Land	Total	Land	Sea Ice
CCSM4	NH	4.2 (6.3)	0.1 (0.1)	2.0 (3.1)	2.2 (3.1)	4.1/2.1 (6.1/3.3)	2.3/1.3 (3.2/1.9)	1.8/0.8 (2.9/1.4)
	SH	3.3 (5.0)	0.9 (1.1)	2.3 (3.9)	0.0 (0.1)	3.2/2.4 (4.9/3.6)	1.0/0.9 (1.2/1.1)	2.2/1.5 (3.7/2.5)
	Global	3.8 (5.7)	0.5 (0.6)	2.1 (3.5)	1.1 (1.6)	3.6/2.2 (5.5/3.4)	1.6/1.1 (2.2/1.5)	2.0/1.2 (3.3/2.0)
CESM1-CAM5	NH	4.6 (5.9)	0.1 (0.2)	2.1 (2.7)	2.4 (3.1)	4.7/2.7 (6.0/3.3)	2.5/1.6 (3.2/2.0)	2.3/1.1 (2.9/1.3)
	SH	3.1 (3.9)	1.1 (1.2)	1.9 (2.7)	0.1 (0.1)	3.7/2.2 (4.9/2.8)	1.2/1.1 (1.3/1.2)	2.6/1.2 (3.6/1.7)
	Global	3.8 (4.9)	0.6 (0.7)	2.0 (2.7)	1.2 (1.6)	4.2/2.5 (5.5/3.1)	1.8/1.3 (2.2/1.6)	2.4/1.1 (3.3/1.5)

[a]All values are negative. Numbers in parenthesis are clear-sky CrRE.
[b]Pairs are (mean of years 2007–2016)/(mean of years 2090–2099).

2.3. Observationally Derived CrRE

We apply observation-based CrRE data from *Flanner et al*. [2011]. This data set is derived from a variety of remote sensing measurements and consists of monthly resolved $1 \times 1°$ resolution Northern Hemisphere (NH) CrRE during 1979–2008. We rederived the observation-based data with two key changes that facilitate a more direct comparison with model output. First, we assume the same snow-free albedos over ice sheets and glaciers as used in CLM. Second, we replace the surface albedo radiative kernels used by *Flanner et al*. [2011] with newly created kernels generated from CCSM4 and CESM1-CAM5, providing consistent cloud conditions for evaluating cryospheric influences from these two models. Kernels were generated using the instantaneous TOM flux changes associated with a +0.01 perturbation in surface albedo, consistent with the method applied by *Shell et al*. [2008].

3. Results/Discussion

3.1. Present-Day CrRE

In the present-day simulations, global annual clear-sky CrRE is -5.7 ± 0.07 W m^{-2} in CCSM4 and -4.9 ± 0.08 W m^{-2} in CESM1-CAM5 (Table 1). In CCSM4 and CESM1, the clear-sky conditions remove the influence of clouds, while including aerosols and gases. The spread represents the interannual standard deviation for each model run. The difference between models is due largely to greater Southern Hemisphere (SH) sea ice cover in CCSM4. The all-sky CrRE in both models is -3.8 (± 0.05 in CCSM4 and ± 0.06 in CESM1-CAM5) W m^{-2}, with the similar magnitudes resulting from greater cloud masking of cryospheric regions in CCSM4 than CESM1-CAM5 (Figure 2, right column). Seasonal variation in CrRE is strongly influenced by the insolation cycle in each hemisphere, with peak NH and SH CrRE occurring in May and November, respectively (Figure 3), about 2 months after peak sea ice extent and 3–4 months after peak snow extent. Sea ice tends to cause the largest effect per unit area due to the darkness of ocean water and contributes 57% and 52% of global all-sky CrRE in CCSM4 and CESM1-CAM5, respectively (Table 1). Snow cover over nonglacial areas contributes 30% and 32% of the global effect in these two models, almost all of it from the Northern Hemisphere. The smaller albedo difference between snow and permanent glaciers results in only 14% and 16% of the effect originating from supraglacial snow (snow atop ice sheets and glaciers), mostly from Antarctica. Total CrRE is larger in the SH, with the majority of SH effect originating from sea ice, whereas NH CrRE is partitioned nearly evenly between snow and sea ice (Table 1). SH supraglacial snow and sea ice contributions are 15% smaller (less negative) and 20% larger (more negative), respectively, in CCSM4 compared with CESM1-CAM5 (Table 1).

Global annual present-day NH model and observation-based CrRE compare well with both CCSM4 and CESM1-CAM5 treatment (Figures 3a and 3b). Using the new CAM4 and CAM5 radiative kernels, annual observationally derived means are -3.9 and -4.6 W m^{-2}, demonstrating influence of different cloud treatments on CrRE. NH model means are larger by 10% and 1% of observation for CCSM4 and CESM1-CAM5, respectively. The high bias in CCSM4 CrRE occurs during March–September and is caused by excessive sea ice. In both models CrRE is more negative than observations over Greenland, the Canadian Arctic Archipelago and most of the Tibetan Plateau, and is less negative over parts of central-eastern Canada and small regions west of the Tibetan Plateau (Figures 4e and 4f). Overly reflective snow on ice sheets, excessive snow cover on the Tibetan Plateau, and excessive sea ice in the North Atlantic may explain some of these discrepancies. The

©2014. American Geophysical Union. All Rights Reserved.

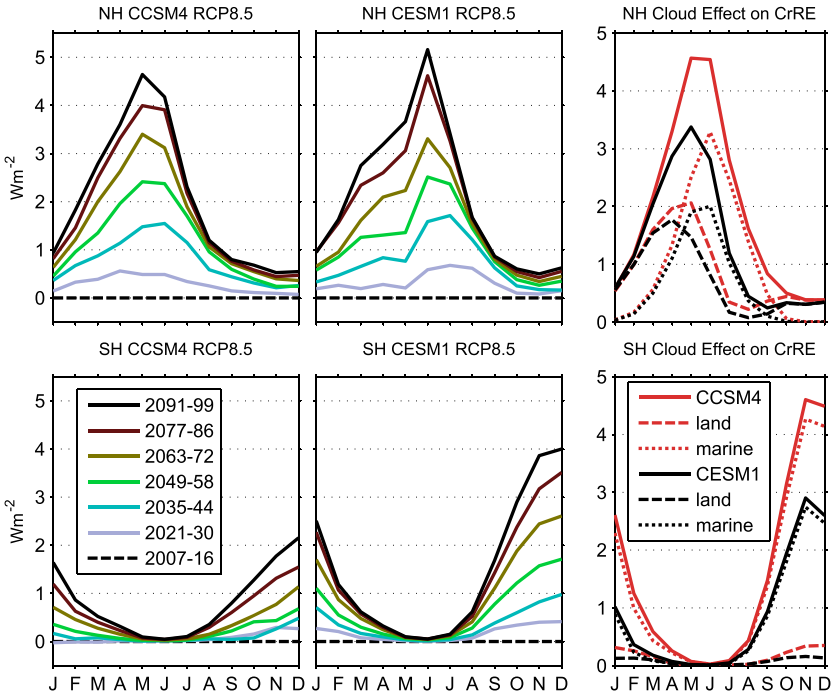

Figure 2. Multidecadal change in (top) Northern and (bottom) Southern Hemispheres' all-sky CrRE simulated in the CCSM4 (Figure 2, left column) and CESM1-CAM5 (Figure 2, middle column) models under the RCP 8.5 scenario. The mean of years 2007–2016 is used as the baseline and subtracted from 10 year averages over different periods. Cloud effects (Figure 2, right column) on present-day CrRE (all-sky conditions minus clear-sky conditions) partitioned into total, land, and marine components. Positive numbers indicate CrRE has become less negative.

contribution of snow may be underestimated over glacial regions, however, because of a higher bare ice albedo assumed in CLM than measured in the ablation zones of Greenland [*Bøggild et al.*, 2010; *Box et al.*, 2012]. Moreover, darkening of snow-free ice surfaces through increased water content is not treated in our modeling but constitutes a fast feedback component of cryospheric albedo change.

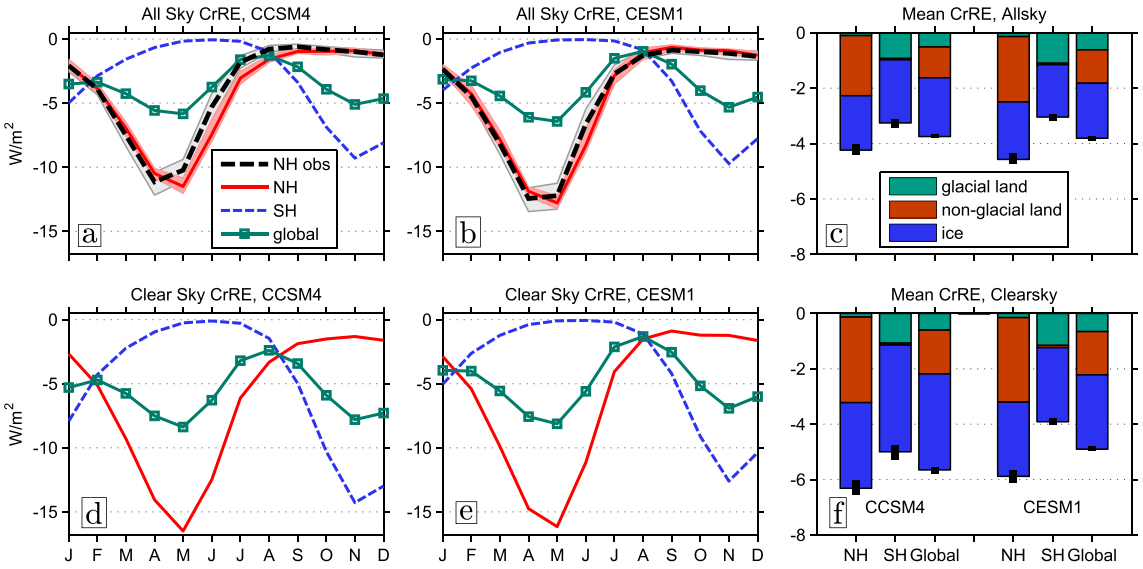

Figure 3. (a–c) All-sky conditions and (d–f) clear-sky conditions, present-day CrRE components simulated with CCSM4 (Figures 3a and 3d) and CESM1-CAM5 (Figures 3b and 3e). Northern Hemisphere (NH) observation-based CrRE from *Flanner et al.* [2011] recalculated using a CAM4 (Figure 3a) and CAM5 (Figure 3b) radiative kernel is also shown. Shading in Figures 3a and 3b indicates full ranges of the NH CrRE in each month. Black bars in Figures 3c and 3f indicate full range of annual-mean CrRE.

©2014. American Geophysical Union. All Rights Reserved.

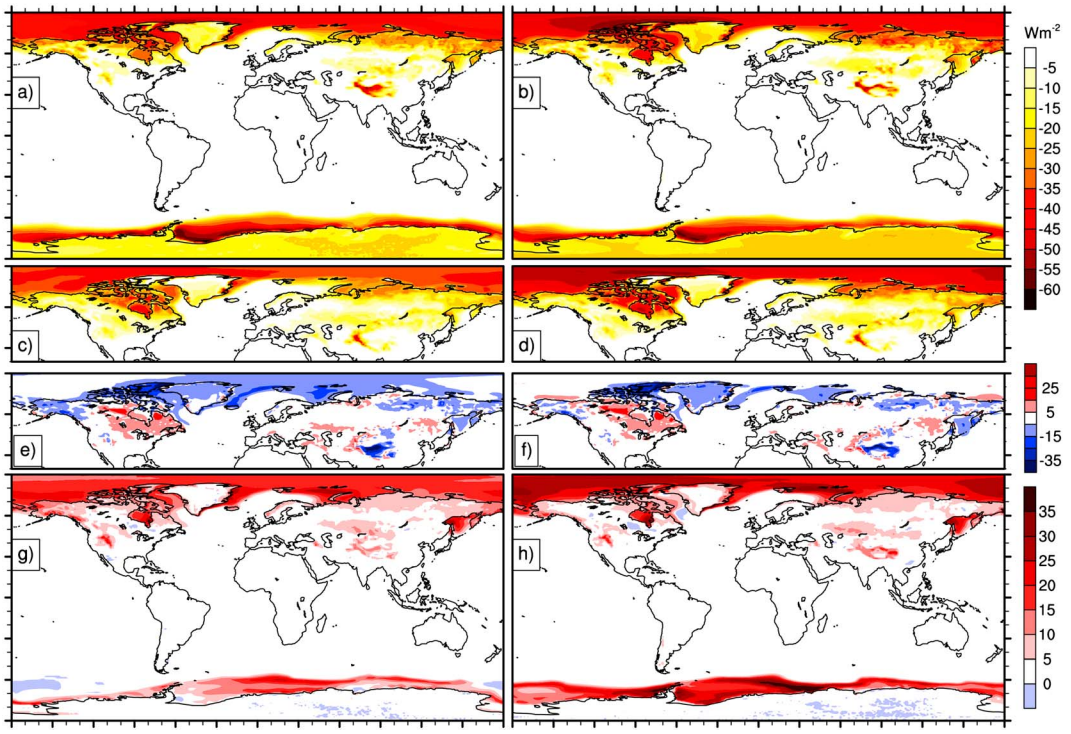

Figure 4. Present-day CrRE simulated using (a) CCSM4 and (b) CESM1-CAM5, along with Northern Hemisphere observations rederived from *Flanner et al*. [2011] using (c) a CAM4 radiative kernel and (d) a CAM5 kernel. (e and f) Model results subtracted by observation. (g and h) Differences between the means of periods 2090–2099 and 2007–2016 of the RCP 8.5 simulations.

Global CrRE increases by 51% in clear-sky conditions compared to all-sky in CCSM4 and by 29% in CESM1-CAM5 (comparing Figures 3c and 3f). Cloud masking on CrRE is largest over sea ice (63% and 35% clear-sky increases in the respective models) and smallest over glacial land (17% and 6% increases). Low Arctic clouds increase automatically with sea ice melting in CAM4 due to a cloud parameterization designed for lower latitudes, resulting in incorrect cloud response to ice melting [*Kay et al*., 2011]. Additionally, clouds in this region are known to be too optically thick in CAM4 and too thin in CAM5 [*Kay et al*., 2012]. These factors result in unrealistic Arctic cloud masking, which also is expected over Antarctic sea ice. Clouds shield cryospheric influence to a lesser extent in these models than the masking of surface albedo anomalies found in previous studies that applied radiative kernels derived from older climate models [*Donohoe and Battisti*, 2011; *Flanner et al*., 2011; *Qu and Hall*, 2013].

CrRE was also evaluated at the surface. Under all-sky conditions, the cryosphere has the effect of increasing global annual surface downwelling solar flux by 1.2 ± 0.02 and 0.9 ± 0.02 W m^{-2} in CCSM4 and CESM1-CAM5, respectively, due to multiple scattering between clouds and the surface. Under clear-sky conditions, both models' downwelling shortwave flux rise by 0.4 ± 0.01 W m^{-2} due to Rayleigh scattering and surface cryosphere albedo.

3.2. Twenty-First Century Evolution of CrRE

We now examine 21st century CrRE changes under the RCP 8.5 forcing scenario. Equilibrium climate sensitivity and 21st century climate response are greater in CESM1-CAM5 compared to CCSM4 [*Meehl et al*., 2013]. The global mean instantaneous shortwave influence of the cryosphere diminishes in magnitude (becoming less negative) by 1.4 ± 0.1 W m^{-2} during the 21st century (mean of years 2090–2099 relative to years 2007–2016) in the CCSM4 experiment, and by 1.8 ± 0.1 W m^{-2} in CESM1-CAM5 (Figure 5, Table 1), or by 38% and 46% of the initial 21st century effect. The boreal land snow, boreal sea ice, and austral sea ice components each contribute between 0.4 and 0.7 W m^{-2} to global CrRE diminishment in both models. Changes are largest around the summer solstice for each hemisphere (Figure 2, left column). The resulting increases in planetary absorbed energy are about 24–31% as large as the change in anthropogenic radiative forcing during this period

©2014. American Geophysical Union. All Rights Reserved.

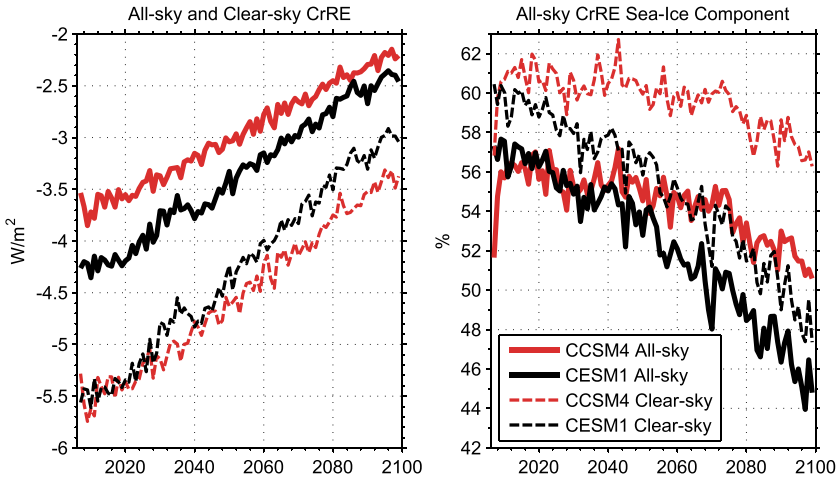

Figure 5. (left) Global annual averages of the all-sky and clear-sky CrRE simulated with CCSM4 and CESM1-CAM5, forced with the RCP 8.5 scenario. (right) The portion of CrRE produced by the presence of sea ice.

(5.7 W m^{-2}) for the RCP8.5 scenario [*Meinshausen et al.*, 2011]. The changes in all-sky and clear-sky CrRE remain mostly steady throughout the 21st century in both the North and South Hemispheres (Figure 5, left), though marine CrRE contribution diminishes more rapidly than terrestrial as sea ice is lost (Figure 5, right). Early 21st century CrRE is more negative in the CESM1-CAM5 RCP 8.5 simulation than in the present-day control simulation (Table 1), caused by differences in shortwave cloud forcing and ice area. Initial CrRE in the CESM1-CAM5 RCP8.5 experiment is also more negative than the CCSM4 version, providing a larger capacity for 21st century change. Under clear-sky conditions, the CCSM4 and CESM1-CAM5 21st century CrRE changes are +2.0 and +2.4 W m^{-2}.

Incorporating global surface temperature change enables an assessment of the global cryospheric albedo feedback, which we find to be $+0.41 \pm 0.06$ W/m^2/K in CCSM4 and $+0.45 \pm 0.04$ W/m^2/K in CESM1-CAM5. These feedback are slightly stronger than the 21st century multimodel mean global albedo feedback of $+0.3 \pm 0.09$ W/m^2/K found by *Winton* [2006] from 12 models used in the Intergovernmental Panel on Climate Change fourth assessment report, but NH cryosphere albedo feedback ($+0.46 \pm 0.04$ and 0.47 ± 0.07 W/m^2/K) are smaller than the 30 year NH feedback of +0.6 W/m^2/K derived from observations during 1979–2008 [*Flanner et al.*, 2011]. Though CESM1-CAM5 has a 29% larger CrRE change over the RCP8.5 experiment than CCSM4, it only has a 10% greater cryospheric feedback, reflecting the larger climate response in CESM1-CAM5.

4. Conclusions

We implement a new diagnostic calculation in CESM of the shortwave cryosphere radiative effect (CrRE), or the exact, instantaneous influence of snow and sea ice on Earth's solar radiation budget. Present-day simulations show that rapidly evolving cryospheric components diminish TOM net solar energy flux by 3.8 W m^{-2} globally, and by 4.2–4.6 W m^{-2} in the Northern Hemisphere, in good agreement with observational assessments. However, CCSM4 exhibits the compensating effects of larger sea ice extent and larger cloud masking of cryospheric surfaces than CESM1-CAM5. CrRE is strongly influenced by the seasonal insolation cycle, and sea ice contributes more to CrRE than terrestrial seasonal snow or glaciers in the present climate. Diminishing cryospheric cover causes global CrRE to decrease (become less negative) by 1.4 and 1.8 W m^{-2}, respectively, in CCSM4 and CESM1-CAM5 RCP8.5 simulations between the beginning and end of the 21st century. Global cryospheric albedo feedback are +0.41 and +0.45 W/m^2/K, indicating that the two models exhibit similar temperature-normalized CrRE change.

Acknowledgments
The authors would like to thank the CESM Polar Climate Working Group for computing resources and support, and Ben Sanderson for helpful discussions. Funding for this work was provided by NSF 1253154 and NASA NNX13AN29G.

References

Arking, A. (1991), The radiative effects of clouds and their impact on climate, *Bull. Am. Meteorol. Soc.*, *71*(6), 795–813.
Bøggild, C. E., R. E. Brandt, K. J. Brown, and S. G. Warren (2010), The ablation zone in northeast Greenland: Ice types, albedos and impurities, *J. Glaciol.*, *56*, 101–113, doi:10.3189/002214310791190776.
Bony, S., et al. (2006), How well do we understand and evaluate climate change feedback processes?, *J. Clim.*, *19*(15), 3445–3482, doi:10.1175/JCLI3819.1.

©2014. American Geophysical Union. All Rights Reserved.

Box, J. E., X. Fettweis, J. C. Stroeve, M. Tedesco, D. K. Hall, and K. Steffen (2012), Greenland ice sheet albedo feedback: Thermodynamics and atmospheric drivers, *Cryosphere*, *6*(4), 821–839, doi:10.5194/tc-6-821-2012.

Briegleb, B., and B. Light (2007), A Delta-Eddington multiple scattering parameterization for solar radiation in the sea ice component of the Community Climate System Model, *NCAR Tech. Note NCAR/TN-472+STR*, doi:10.5065/D6B27S71.

Donohoe, A., and D. S. Battisti (2011), Atmospheric and surface contributions to planetary albedo, *J. Clim.*, *24*(16), 4402–4418, doi:10.1175/2011JCLI3946.1.

Flanner, M. G., C. S. Zender, J. T. Randerson, and P. J. Rasch (2007), Present-day climate forcing and response from black carbon in snow, *J. Geophys. Res.*, *112*, D11202, doi:10.1029/2006JD008003.

Flanner, M. G., K. M. Shell, M. Barlage, D. K. Perovich, and M. A. Tschudi (2011), Radiative forcing and albedo feedback from the Northern Hemisphere cryosphere between 1979 and 2008, *Nat. Geosci.*, *4*(3), 151–155, doi:10.1038/ngeo1062.

Gent, P. R., et al. (2011), The Community Climate System Model Version 4, *J. Clim.*, *24*(19), 4973–4991, doi:10.1175/2011JCLI4083.1.

Holland, M. M., D. A. Bailey, B. P. Briegleb, B. Light, and E. Hunke (2012), Improved sea ice shortwave radiation physics in CCSM4: The impact of melt ponds and aerosols on Arctic Sea Ice, *J. Clim.*, *25*(5), 1413–1430, doi:10.1175/JCLI-D-11-00078.1.

Hurrell, J. W., et al. (2013), The Community Earth System Model: A framework for collaborative research, *Bull. Am. Meteorol. Soc.*, *94*(9), 1339–1360, doi:10.1175/BAMS-D-12-00121.1.

Kay, J. E., K. Raeder, A. Gettelman, and J. Anderson (2011), The boundary layer response to recent Arctic sea ice loss and implications for high-latitude climate feedbacks, *J. Clim.*, *24*(2), 428–447, doi:10.1175/2010JCLI3651.1.

Kay, J. E., M. M. Holland, C. M. Bitz, E. Blanchard-Wrigglesworth, A. Gettelman, A. Conley, and D. Bailey (2012), The influence of local feedbacks and northward heat transport on the equilibrium Arctic climate response to increased greenhouse gas forcing, *J. Clim.*, *25*(16), 5433–5450, doi:10.1175/JCLI-D-11-00622.1.

Lawrence, D. M., et al. (2011), Parameterization improvements and functional and structural advances in Version 4 of the Community Land Model, *J. Adv. Model. Earth Syst.*, *3*(3), 1–27, doi:10.1029/2011MS000045.

Meehl, G. A., W. M. Washington, J. M. Arblaster, A. Hu, H. Teng, J. E. Kay, A. Gettelman, D. M. Lawrence, B. M. Sanderson, and W. G. Strand (2013), Climate change projections in CESM1(CAM5) compared to CCSM4, *J. Clim.*, *26*(17), 6287–6308, doi:10.1175/JCLI-D-12-00572.1.

Meinshausen, M., et al. (2011), The RCP greenhouse gas concentrations and their extensions from 1765 to 2300, *Clim. Change*, *109*(1–2), 213–241, doi:10.1007/s10584-011-0156-z.

Qu, X., and A. Hall (2013), On the persistent spread in snow-albedo feedback, *Clim. Dyn.*, *42*, 69–81, doi:10.1007/s00382-013-1774-0.

Ramanathan, V., R. D. Cess, E. F. Harrison, P. Minnis, B. R. Barkstrom, E. Ahmad, and D. Hartmann (1989), Cloud-radiative forcing and climate: Results from the Earth radiation budget experiment, *Science*, *243*(4887), 57–63, doi:10.1126/science.243.4887.57.

Shell, K. M., J. T. Kiehl, and C. A. Shields (2008), Using the radiative kernel technique to calculate climate feedbacks in NCAR's Community Atmospheric Model, *J. Clim.*, *21*(10), 2269–2282, doi:10.1175/2007JCLI2044.1.

Soden, B. J., and I. M. Held (2006), An assessment of climate feedbacks in coupled ocean–atmosphere models, *J. Clim.*, *19*(14), 3354–3360, doi:10.1175/JCLI3799.1.

Soden, B. J., I. M. Held, R. Colman, K. M. Shell, J. T. Kiehl, and C. A. Shields (2008), Quantifying climate feedbacks using radiative kernels, *J. Clim.*, *21*(14), 3504–3520, doi:10.1175/2007JCLI2110.1.

Stephens, G. (2005), Cloud feedbacks in the climate system: A critical review, *J. Clim.*, *18*, 237–273.

Winton, M. (2006), Amplified Arctic climate change: What does surface albedo feedback have to do with it?, *Geophys. Res. Lett.*, *33*, L03701, doi:10.1029/2005GL025244.

©2014. American Geophysical Union. All Rights Reserved.